INDIAN JOURNAL OF SCIENCE AND TECHNOLOGY

RESEARCH ARTICLE

Optical Properties of AgNPs and $BiPO_4$:Pr(III) Phosphor and Comparative Studies of Albumins (Local Eggs, Mizoram)

N Mohondas Singh[1]*, Fidelia Lalrindiki[1]

1 Department of Chemistry, School of Physical Sciences, Mizoram University, Aizawl, 796004, India

OPEN ACCESS

Received: 23-01-2023

Accepted: 09-06-2023

Published: 13-09-2023

Citation: Singh NM, Lalrindiki F (2023) Optical Properties of AgNPs and $BiPO_4$:Pr(III) Phosphor and Comparative Studies of Albumins (Local Eggs, Mizoram). Indian Journal of Science and Technology 16(SP1): 165-173. https://doi.org/10.17485/IJST/v16sp1.msc23

* **Corresponding author**.

nmdas08@rediffmail.com

Funding: None

Competing Interests: None

Published By Indian Society for Education and Environment (iSee)

ISSN
Print: 0974-6846
Electronic: 0974-5645

Abstract

Objectives: This work investigated the photoluminescence behaviour of Pr^{3+}-doped $BiPO_4$ phosphors synthesised by the co-precipitation method, and the combination of albumin with AgNPs shows the development of the FRET mechanism. **Methods:** Pr^{3+}-doped $BiPO_4$ phosphors were synthesised by the co-precipitation method, and AgNPs were prepared by the reduction method. The prepared phosphors were characterised by XRD, SEM, FT-IR, UV-vis, and PL spectroscopy techniques. The activity of proteins in the mixing of phosphors and AgNPs was studied through the PL study, leading to the formation of the FRET mechanism. **Findings:** A monoclinic phase was observed through XRD and FT-IR studies; however, the SEM image showed the agglomeration of the nanoparticles of phosphors. The bands were observed at the 670-750 nm for the emission spectra produced at $^3P_1 \rightarrow {}^3F_4$ and $^3P_0 \rightarrow {}^3F_4$ transitions, and they were obtained as excitation spectra at $^3P_{0,1,2}$ in 468.6 nm via the photoluminescence study. The decay time of the prepared phosphors was also investigated, with the calculated average lifetime for Pr^{3+} (7 at.%) being 0.14572 and the goodness of fit (R^2) for the concentration being 0.98939. The CIE chromaticity diagram revealed a nearly white colour emission upon excitation at 468.6 nm. The prepared phosphors may be useful for solid-state lighting. Meanwhile, taking two different types of albumin to show which one got further intensity when mixed with phosphor material and a silver nanoparticle for enhancing the intensity of the mixed sample also shows energy transfer between the excitation and emission spectra of the prepared sample by using a basic FRET mechanism. **Novelty:** According to the author's knowledge, no comprehensive work was dedicated to the objective of this research. The comparison of albumins of duck and local eggs (Mizoram, India) with phosphors and AgNPs was not shown anywhere, where it will be more applicable in the field of phosphor. Therefore, it is sensible to modify the materials to improve the FRET mechanism for fulfilling the potential of this work.

Keywords: Phosphors; PL; AgNPs; Emission; Excitation spectra

1 Introduction

One of the contemporary era's fastest-growing technologies, nanotechnology has emerged as a key tool for producing sophisticated materials. Due to their tiny size, high surface area to volume ratio, a high number of weakly linked bonds, and the presence of unsaturated atoms on the surface, nano-sized materials had physical and chemical properties that were quite different from equivalent bulk materials. Ag-NP localised plasmon effects were used to exhibit photoluminescence enhancement in rare-earth ion-doped glass based on GeO_2. Numerous photonic applications have been proven for this host doped with rare-earth ions and metallic NPs, which also serve as the inspiration for the current work[1,2]. Additionally, they have beneficial qualities, including decreased light dispersion and concentrated surface flaws, etc.[3]. Quantum dots and other nanomaterials with diameters smaller than 10 nm are also popular topics of study because of their exceptional optical and physicochemical characteristics and diverse range of uses. Some AgNP-containing compounds showed longer fluorescence lifetimes than only AgNP-free complexes[4–6]. ZnO, TiO_2, and CuO nanoparticles have received a lot of attention in recent years due to their outstanding performance in a variety of sectors, including photocatalysis, sensors, quantum dots, bio-medical applications, and others[7,8].

Inorganic phosphor materials with rare earth ion doping have been shown to have used in a variety of domains, including solid-state physics, photochemistry, biophysics, etc.[9]. These materials are made up of two parts: a host material and an activator, the latter of which is a doping rare earth ion[10]. Phosphate-based materials have been chosen as one of the finest hosts among the many host materials because of their strong physicochemical and thermal stability[11]. $BiPO_4$ is a member of the phosphate family and possesses many intriguing properties, including a high absorption edge, high mechanical and chemical stability, and similar ionic sizes to those of Bi^{3+} and lanthanide ions. It also has numerous potential applications in a variety of industries, including ion sensing, catalysts, radioactive element separation, etc.[12]. Additionally, three alternative crystallographic forms of $BiPO_4$ can occur, including hexagonal, low-temperature monoclinic and high-temperature monoclinic. In a monoclinic phase, the Bi^{3+} ion is surrounded by nine oxygen atoms, as opposed to eight in a hexagonal configuration. According to numerous researchers, the monoclinic low-temperature structure of $BiPO_4$ exhibits the strongest luminous property when compared to other phases. A phosphor's luminescent quality is highly influenced by its phase structure. Since the 4f electrons of rare earth ions are shielded by 6s and 5p orbitals, the f-f electronic transitions of rare earth ions are not affected by the external environment, producing sharp absorption and emission bands.

In lanthanide ion-doped luminescent materials, the luminescence property is typically originated from the electronic transition within the doped lanthanide ions' 4f electrons. Varied rare earth ions were doped into the host lattice, and this resulted in different emission colours. For instance, the ion doping of Ce^{3+}, Eu^{3+}, and Sm^{3+} often emits blue, red, and orange colours, respectively[13]. Due to the Tb^{3+} ion's electronic transition to state $^5D_4 \rightarrow {}^7F_5$, trivalent terbium ions typically have a green colour. And it might be used in a variety of industries, such as lighting, display, décor, and traffic signals[14]. Additionally, it is a part of white light. Therefore, using ethylene glycol as the reaction medium, the current study examined the luminous characteristics of Tb^{3+} ion-doped $BiPO_4$ synthesised via co-precipitation. The effect of Tb^{3+} ion concentration has been studied to achieve optimal emission since the doping ion concentration has a significant impact on the luminescence property. To the author's knowledge, no paper that is similar to our work has been published yet.

2 Methodology

To ascertain the crystal structure and phase composition of the generated samples, Bruker AXS, and D8 Focus-Powder XRD were utilised. Shimadzu's SHIMADZU CORP.00703 FT-IR spectrometer was used to record the vibrational spectra. To determine the morphology of the prepared sample, a JEOL-JSM-6390LV instrument was used. Using 150 W xenon lamps as excitation light sources, the Fluorescence Spectrophotometer F-7000 recorded the photoluminescence excitation, emission, and decay times. Every measurement was carried out at room temperature.

Local Eggs and Duck eggs (Mizoram, India) were collected for extracting the albumins.

Various methods have been reported for the synthesis of the phosphors such as molten salt, solid-state reaction, co-precipitation, reflux method, hydrothermal process, microemulsion, thermolysis, sol-gel, Ostwald ripening process etc. But, a wet chemical method has many advantages over a solid-state reaction in terms of particle homogeneity, low power consumption and time factor. For this study, the phosphors will be synthesized using co-precipitation, since they are one of the simplest and most effective methods and yet has high yield and high product purity and easily reproducible and have many advantages over solid-state reaction method in terms of temperature requirement and homogeneity of the products formed. Therefore, in the case of the co-precipitation method, the reaction is taking place in a liquid state; therefore, the temperature required is low as compared to the solid-state reaction method.

2.1 Silver nanoparticle synthesis

A large excess of $NaBH_4$ was needed to stabilise the created silver nanoparticles and reduce the ionic silver. Different amounts of 0.001 M silver nitrate were added dropwise to 30 mL of a cool 0.002 M sodium borohydride solution (1 drop per second). The reaction mixture was vigorously stirred on a magnetic stirrer. The solution turned light yellow following the addition of 2 mL of silver nitrate, and it turned brighter yellow after the addition of all of the silver nitrate[15].

2.2 Synthesis of Pr^{3}+-doped $BiPO_4$

For the synthesis of $BiPO_4:Pr^{3+}$, the phosphor was made by mixing the stoichiometric amount of $Bi(NO_3)_3.5H_2O$ with 70 ml of ethylene glycol in a flask with a flat bottom. Stoichiometric proportions of $NH_4H_2PO_4$ and $PrCl_3.H_2O$ were added to this solution, and it was firmly shaken to dissolve the crystals. After that, the mixture was stirred at 170°C for two hours. The obtained white precipitate was centrifuged, and then it went through about five cycles of distilled water washing before being cleaned with acetone. The sample was then dried in an oven for a further 12 hours at 80°C[16].

3 Results and Discussion

3.1 XRD Study

Figure 1 displays the most instructive portion of the $BiPO_4:Pr^{3+}$ (7 at.%) sample's XRD patterns. These graphs demonstrate that the prepared sample had a low monoclinic phase following the requirements of the standard JCPDS card number 15-0767. Impurities in the sample may be the cause of the peak at 2θ degrees in the diffraction pattern of the 7at.% Pr^{3+}-doped $BiPO_4$ sample[17]. Because it is difficult to see the monoclinic phase in the high-temperature annealed sample, no impurity peak was seen. If we add and compare the as-prepared sample to the annealed sample, it will become apparent that the peak intensity may grow and the bandwidth may also shrink as the annealing temperature rises, which also suggests that the crystallinity will rise. There have also been reports of this kind of phase transition at annealing temperatures in the literature[18].

3.2 FT-IR and SEM Study

$BiPO_4:Pr^{3+}$ (7 at.%) produced sample Figure 2 was examined in an infrared spectrophotometer. The sample revealed that the peaks centring at around 3317.56 cm^{-1} related to the bending and stretching vibrations of adsorbed water molecules. The distinctive bands of PO_4^{3-} are those seen between 400 cm^{-1} and 1064.71 cm^{-1}. The O-P-O linkage's stretching symmetric vibrations are responsible for the bands seen at 910.40, 948.98, and 987.55 cm^{-1}, while the bending vibrations of the O-P-O linkage are responsible for the bands seen at 524.64, 547.78, and 601.79 cm^{-1}. The bands that may be seen are those that are typical of the monoclinic structure of the PO_4^{3-}group. This FT-IR analysis thus provided support for the establishment of a monoclinic structure in the material[16].

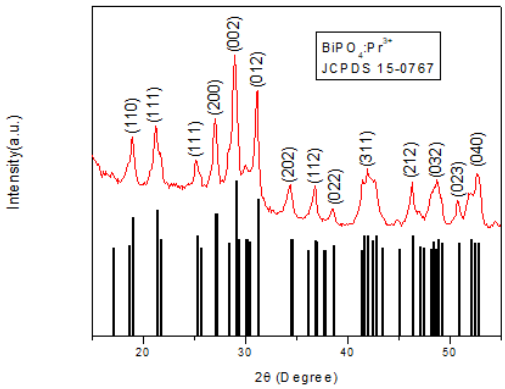

Fig 1. XRD patterns of a prepared sample of $BiPO_4:Pr^{3+}$ (7at.%)

The morphology of samples is examined using the scanning electron microscope picture. Figure 3 displays the SEM picture of the synthesised $BiPO_4:Pr^{3+}$ (7at.%). Because of agglomeration, it is seen that no distinct shape is obtained and the particles are larger. Calculations from Figure 3(**a**) reveal that the average SEM image is 196.42857 nm.

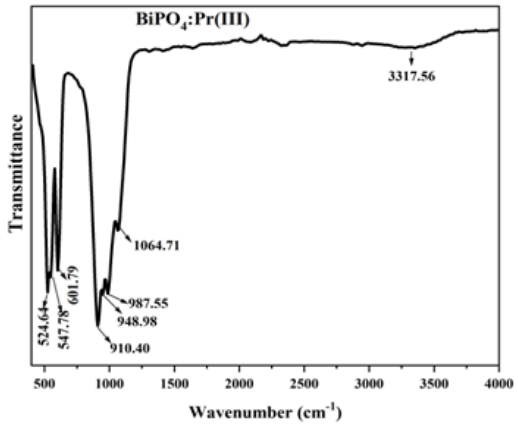

Fig 2. FT-IR spectrum of $BiPO_4:Pr^{3+}$ (7 at.%)

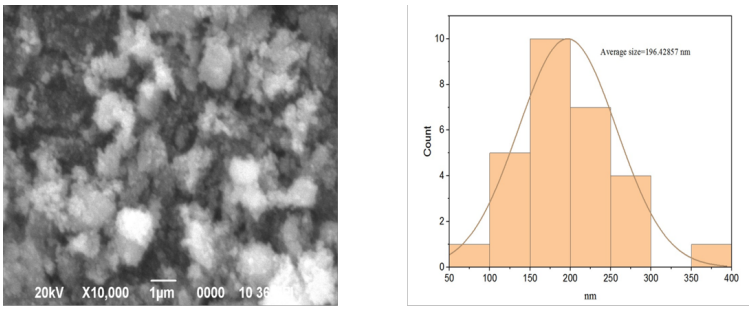

Fig 3. (a) SEM image of $BiPO_4:Pr^{3+}$ (7 at.%); (b) Calculated average SEM image of the prepared sample

3.3 Photoluminescence Study:

In Figure 4 **(a),** the 350–500 nm spectral range of the $BiPO_4:Pr^{3+}$ photoluminescence's excitation spectra are shown. The spectra were obtained by measuring the luminescence at different wavelengths (nm), and they contain lines associated with transitions from the ground $^3H_4$ level to the three $P_{0,1,2}$ multiplet of the Pr^{3+} ion. The PL spectra of Pr^{3+}-doped $BiPO_4$ samples under direct excitation are displayed inFigure 4(**b**). In the vicinity of 570–600 nm, where $^1D_2 \rightarrow {}^3H_4$ is created roughly, the $^3P_0 \rightarrow {}^3H_6$ transition is often expected to form and overlap the $^1D_2 \rightarrow {}^3H_4$ transition level. In the 670–750 nm region, $^3P_1 \rightarrow {}^3F_4$ and $^3P_0 \rightarrow {}^3F_4$ transitions are seen, and their amplitudes grow as the concentration of the Pr^{3+} ion rises, since the rare earth content affects PL spectra.

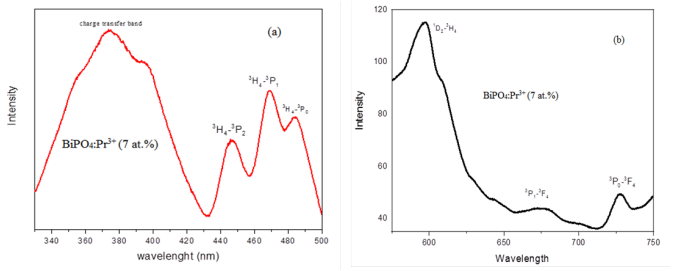

Fig 4. (a) PL spectra of Pr^{3+}-doped $BiPO_4$ λ_{em}=611nm and (b) PL spectra of Pr^{3+}-doped $BiPO_4$ λ_{ex}=468nm

The photoluminescence spectra of AgNPs combined with both Zo and Duck eggs albumin as well as with $BiPO_4:Pr^{3+}$ are presented in Figure 5 **(a-d)** and Figure 6. Here, the luminescence characteristic of $BiPO_4:Pr^{3+}$ is also measured. The spectral range is 300–500 nm, and the excitation peak of $BiPO_4:Pr^{3+}$ mixed with AgNPs was first seen at 315 nm. Protein was then added to the mixture of AgNPs and $BiPO_4:Pr^{3+}$, and the amount and concentration of the mixture are 1:2:1 for $BiPO_4:Pr^{3+}$, AgNPs, and protein albumin of Zo egg (local egg, Mizoram), and Duck egg, respectively. Their excitation spectra span a variety of wavelengths, such as 337 nm for an AgNPs and duck albumin mixture. When $BiPO_4:Pr^{3+}$ is once more involved, the intensity rises. When duck egg albumin was involved, the intensity was much higher when Zo egg was supplied, yet the excitation peak was found at a range between 325 and 350 nm, which is practically identical to that of duck egg albumin. Figure 10 displays the overlay of the spectra that were acquired for various types of combinations.

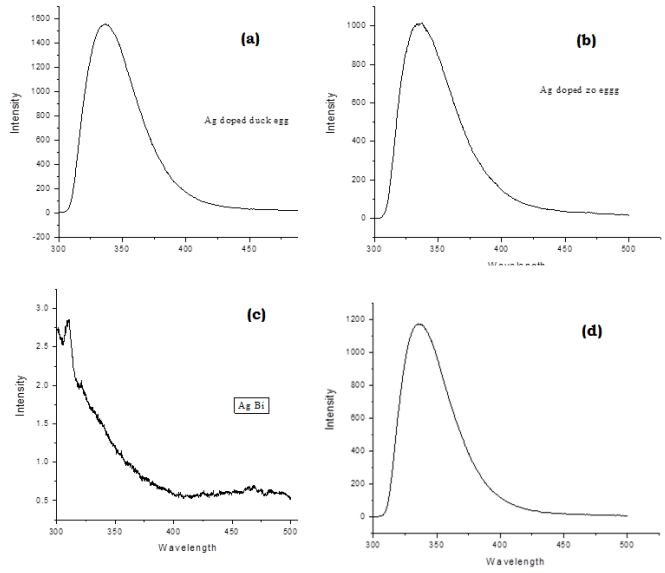

Fig 5. (a) PL Spectra of AgNPs mixed with $BiPO_4$:Pr(III) and duck egg albumin, (b) PL Spectra of AgNPs mixed with $BiPO_4$:Pr(III) and Zo egg albumin (local egg, Mizoram), (c) PL spectra of AgNPs and $BiPO_4$:Pr(III) and (d) PL spectra of Ag NP mixing with Albumin of Duck egg

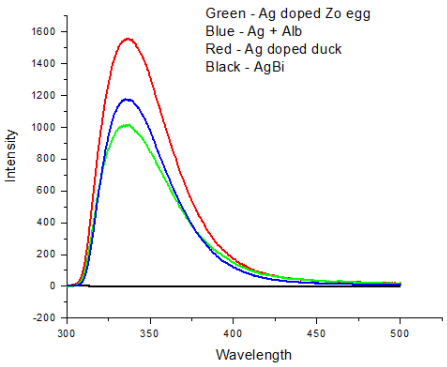

Fig 6. Overlay spectra of Figure 5 (a-d)

3.4 Lifetime Study

The Pr^{3+} ion-doped $BiPO_4$ phosphors have been produced, and their luminescence decay curves have been assessed. The excitation and emission wavelengths were set to 468 and 611 nm, respectively, for all concentrations, to measure the decay curves. Figure 7 displays the calculated decay curves. According to Devi *et al.*, the bi-exponential equation provides a good fit for the observed degradation curves.

$I=I_1 \exp(-t/\tau_1)+I_2\exp(-t/\tau_2)$

Here, the intensities at two different time intervals, I_1 and I_2, are represented by the letters I_1 and I_2, while their respective decay durations, τ_1 and τ_2, are also shown. The non-homogeneous distribution of dopant ions into the host lattice, energy transfer from the donor atom, defects in the host and the existence of impurities, and the bi-exponential curve fitting of a phosphor all affect how it decays [19]. Using the following equation, the average decay time may be calculated:

$\tau_{ave} = (I_1\tau_1^2 +I_2\tau_2^2)/(I_1\tau_1+I_2\tau_2)$

The average lifetime for the Pr^{3+} 7 at.% is calculated to be 0.14572, and the goodness of fitting (R^2) for the concentration is determined to be 0.98939.

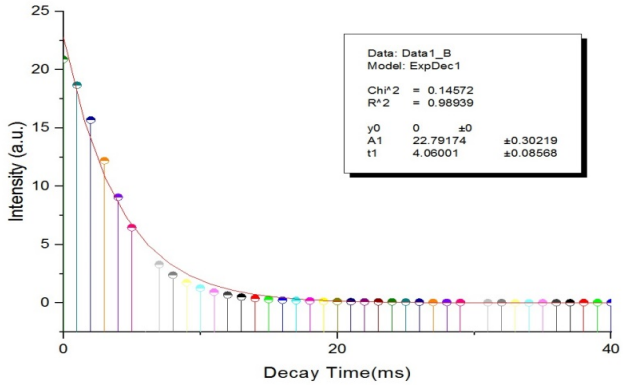

Fig 7. Photoluminescence decay curve of $BiPO_4$:Pr(III)

3.5 CIE Study

The coordinates that determine the perceived emission colour of a phosphor were revealed in the Commission International de L' Eclairage (CIE) chromaticity diagram [19–21]. The emission spectra of the phosphors were used to calculate their colour coordinates, and Table 1 shows the associated co-related colour temperatures. The following is Mc Camy's equation [17].

$CCT= -473n^3 +3601n^2-6861n+5514.31$ and $n=(x-x_e)/(y-y_e)$

CIE chromaticity coordinates and CCT of the $BiPO_4$:Pr^{3+} (7 at. %) phosphors upon excitation at 468.6 nm, where the x and y are the calculated colour coordinates. The CIE chromaticity diagrams for the as-prepared sample (7at % Pr^{3+}-doped $BiPO_4$)

Table 1. The associated co-related colours

X	Y	Z	x	y
695.255	573.131	1739.071	0.231	0.191

upon excitation at 468.6nm are shown in Figure 8. This diagram showed that the samples showed bluish-purple colour emission.

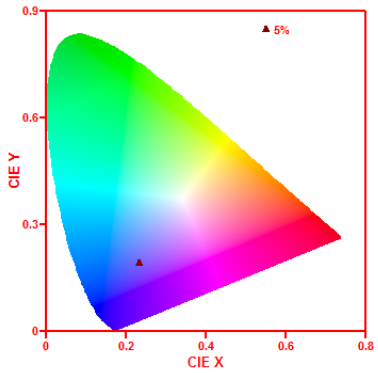

Fig 8. CIE chromaticity diagram for an as-prepared sample of $BiPO_4$:Pr^{3+} (7at.%)

3.6 FRET Mechanism Study

As shown in Figure 9 **,** the excitation and emission spectra of duck albumin were combined with AgNPs to observe the PL spectroscopy. The donor and acceptor of the sample were observed to overlap each other, giving peaks of 237 nm and 273 nm, indicating that they were in very close proximity, indicating that the FRET is a distance-dependent process where the resonant energy is transferred. The efficacy of the FRET mechanism may be increased because the interaction between the donor-acceptor fluorophore of the protein and Pr^{3+}-doped $BiPO_4$ luminous nanoparticles results in changes to their lifetimes due to the presence of the metal core silver nanoparticle. By boosting or decreasing the energy transfer between the donor-acceptor fluorophore molecule and the silver nanoparticle, the presence of the silver nanoparticle reduces the lifetime when it was coupled to the doped particle [5].

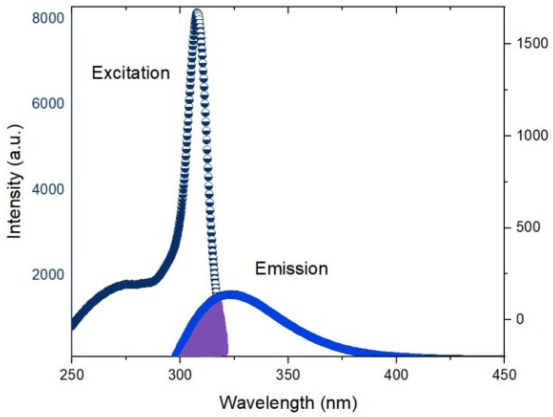

Fig 9. Spectral overlap between the excitation and emission of AgNPs mixed with Duck egg albumin

4 Conclusion

$BiPO_4:Pr^{3+}$, the host of the rare earth-doped luminous nanoparticle we obtained, was successfully doped. Our generated sample is a low-temperature monoclinic structure with a bluish-purple colour in the CIE diagram, as is evident from the data acquired from the absorption spectra, the Fourier transform-infrared spectrum, the XRD diagram, and luminescence spectroscopy. The image of the sample is also examined with the scanning electron microscope (SEM), where we can see its morphology but it is not well portrayed due to agglomeration. However, based on calculations, the size of the particle was determined to be 196.43 nm.

The basic FRET mechanism between the proteins combined with the AgNPs and $BiPO_4:Pr^{3+}$ phosphor was effectively observed. We found that the constructed overlapped excitation and emission spectra of the sample demonstrated that the sample's distance dependence is a result of the FRET mechanism, which can also result in the development of resonance energy transfer.

When prepared, the silver nanoparticles observed using the reduction process displayed a yellow colour and provided a pleasant and good peak of absorption at 409 nm when observed using UV-visible spectroscopy.

$BiPO_4:Pr^{3+}$ combining with albumins and AgNPs is a new thing where no similar works were shown, which is also a new application in the field of phosphors. Local eggs from Mizoram, India and Duck eggs were also never seen compared in this field where the albumins content was measured with the use of Photoluminescence Spectroscopy and useful in the calculation of a basic FRET mechanism. This type of work can be expanded by using a lot of comparisons with different types of albumins. With the help of the enhancing property of AgNPs the work obtained is more suitable and applicable in this field. The current work will be suitable and applicable using different hosts and different metallic NPs.

5 Declaration

Presented in 4th Mizoram Science Congress (MSC 2022) during 20th & 21st October 2022, organized by Mizoram Science, Technology and Innovation Council (MISTIC), Directorate of Science and Technology (DST) Mizoram, Govt. of Mizoram in collaboration with science NGOs in Mizoram such as Mizo Academy of Sciences (MAS), Mizoram Science Society (MSS), Science Teachers' Association, Mizoram (STAM), Geological Society of Mizoram (GSM), Mizoram Mathematics Society (MMS), Biodiversity and Nature ConservationNetwork (BIOCONE) and Mizoram Information & Technology Society (MITS). The Organizers claim the peer review responsibility.

References

1) Bordon CDDS, Dipold J, Wetter NU, De Rossi W, Freitas AZ, Kassab LRP. Effect of Silver Nanoparticles on the Optical Properties of Double Line Waveguides Written by fs Laser in Nd3+-Doped GeO2-PbO Glasses. *Nanomaterials*. 2023;13(4):1–13. Available from: https://doi.org/10.3390/nano13040743.
2) Hong NH. Introduction to Nanomaterials: Basic Properties, Synthesis, and Characterization. *Nano-Sized Multifunctional Materials*. 2019;1:1–19.
3) Khan I, Saeed K, Khan I. Nanoparticles: Properties, applications and toxicities. *Arabian Journal of Chemistry*. 2019;12(7):908–931. Available from: https://doi.org/10.1016/j.arabjc.2017.05.011.
4) Joshi PN, Mathias A, Mishra A. Synthesis of ecofriendly fluorescent carbon dots and their biomedical and environmental applications. *Materials Technology*. 2018;33(10):672–680. Available from: https://doi.org/10.1080/10667857.2018.1492683.
5) Bayan S, Gogurla N, Ghorai AKS, Ray SK. Förster Resonance Energy Transfer Mediated Charge Separation in Plasmonic 2D/1D Hybrid Heterojunctions of Ag–C₃N₄/ZnO for Enhanced Photodetection. *ACS Applied Nano Materials*. 2019;2(6):3848–3856. Available from: https://doi.org/10.1021/acsanm.9b00705.
6) Saiga K, Haraguchi T, Kitahama Y, Hosokai T, Matsuzaki H, Moon D, et al. Optical Properties of Chiral Azo-Schiff Base Mn(II) and Zn(II) Complexes with Silver Nanoparticles. *Journal of Materials Science and Chemical Engineering*. 2021;9(4):1–10. Available from: https://doi.org/10.4236/msce.2021.94001.
7) Song T, Qu Y, Ren Z, Yu S, Sun M, Yu X, et al. Synthesis and Characterization of Polyvinylpyrrolidone-Modified ZnO Quantum Dots and Their In Vitro Photodynamic Tumor Suppressive Action. *International Journal of Molecular Sciences*. 2021;22(15):1–14. Available from: https://doi.org/10.3390/ijms22158106.
8) Venkatasubramanian R, Srivastava RS, Misra RDK. Comparative study of antimicrobial and photocatalytic activity in titania encapsulated composite nanoparticles with different dopants. *Materials Science and Technology*. 2008;24(5):589–595. Available from: https://doi.org/10.1179/174328408X282065.
9) Cho U, Chen JK. Lanthanide- Based Optical Probes of Biological Systems. *Cell Chemical Biology*. 2020;27(8):921–936. Available from: https://doi.org/10.1016/j.chembiol.2020.07.009.
10) Xu S, Li P, Wang Z, Li T, Bai Q, Sun J, et al. Luminescence and energy transfer of Eu2+/Tb3+/Eu3+ in LiBaBO3 phosphors with tunable-color emission. *Journal of Materials Chemistry C*. 2015;3(35):9112–9121. Available from: https://doi.org/10.1039/C5TC01577D.
11) Shi X, Liu Y, Zhang J, Zhang K, Li P, Zuo H, et al. Effects of pH and Sm3+ doping on the structure, morphology and luminescence properties of BiPO4:Sm3+ phosphors prepared by hydrothermal method. *Ceramics International*. 2015;41(2 (Part B)):3162–3168. Available from: https://doi.org/10.1016/j.ceramint.2014.10.164.
12) Naidu BS, Vishwanadh B, Sudarsan V, Vatsa RK. BiPO4: A better host for doping lanthanide ions. *Dalton Transactions*. 2012;41(11):3194–3203. Available from: https://doi.org/10.1039/C2DT11944G.

13) Sharma RK, Ghosh P. Lanthanide-Doped Luminescent Nanophosphors via Ionic Liquids. *Frontiers in Chemistry*. 2021;9:1–26. Available from: https://doi.org/10.3389/fchem.2021.715531.
14) Huang M, Xu Z, Hou C, Jia HLL, Sun J, Guan M. Facile synthesis of colloidal photoluminescent BiPO4:Ln (Eu,Tb) nanoparticles well-dispersed in polar solvents. *CrystEngComm*. 2019;21(2):278–282. Available from: https://doi.org/10.1039/C8CE01363B.
15) Rashid MU, Bhuiyan MKH, Quayum ME. Synthesis of Silver Nano Particles (Ag-NPs) and their uses for Quantitative Analysis of Vitamin C Tablets. *Dhaka University Journal of Pharmaceutical Sciences*. 2013;12(1):29–33. Available from: https://doi.org/10.3329/dujps.v12i1.16297.
16) Naorem RS, Singh NP, Singh NM. Photoluminescence properties of Tb3+ doped BiPO4 nanophosphor synthesised by co-precipitation method using ethylene glycol. *Materials Technology*. 2022;37(8):610–617. Available from: https://doi.org/10.1080/10667857.2020.1866919.
17) Naorem RS, Singh NP, Singh NM. Photoluminescence studies of Ce3+ ion-doped BiPO4 phosphor and its photocatalytic activity. *International Journal of Applied Ceramic Technology*. 2020;17(6):2744–2751. Available from: https://doi.org/10.1111/ijac.13600.
18) Devi CV, Phaomei G, Yaiphaba N, Singh NR. Luminescence behavior of YVO4: Dy3+ phosphors with enhanced photoluminescence on co-doping Bi3+ ions. *Journal of alloys and compounds*. 2014;583:259–266. Available from: https://doi.org/10.1016/j.jallcom.2013.08.139.
19) Sharma KG, Singh NR. Synthesis and luminescence properties of CaMO4: Dy3+(M = W, Mo) nanoparticles prepared via an ethylene glycol route. *New Journal of Chemistry*. 2013;37(9):2784–2791. Available from: https://doi.org/10.1039/C3NJ00155E.
20) Singh NP, Singh NR, Singh NM. Synthesis of CdMoO4:Sm3+ phosphors at room temperature and investigation on photoluminescence properties. *Optik*. 2018;156:365–373. Available from: https://doi.org/10.1016/j.ijleo.2017.11.045.
21) Ramananda SN, Singh NP, Brojendro SS, Singh NH, Jogat G, Singh NM. Effect of annealing temperatures on the structural and photoluminescence properties of Tb3+ ions doped BiPO4 nanophosphors. *Materials Technology*. 2022;37(12):2289–2299. Available from: https://doi.org/10.1080/10667857.2022.2029289.